Global Scientific JOURNALS
GSJ: Volume 8, Issue 4, April 2020, Online: ISSN 2320-9186
www.globalscientificjournal.com

AUTOMATIC BRAIN TUMOR DETECTION AND FEATURE EXTRACTION FROM MRI IMAGE

Md. Ahasan Kabir

Dept. of Electronics and Telecommunication Engineering
Chittagong University of Engineering and Technology
Chittagong, Bangladesh
kabir.ece07@gmail.com

KeyWords
MRI, Brain Tumor, Stastical Feature, Chan-Vese algorithm, Image Enhancement, Anisotropic diffusion process,

ABSTRACT

The brain tumor is one of the major dangerous health problems. Early detection and diagnosis of brain tumors reduce the mortality rate significantly. For efficient detection and classification, this paper has proposed an automatic brain tumor detection and classification algorithm. The proposed algorithm divided into five steps. At first, the input MRI image is preprocessed using principle component-based grayscale conversion coupled with anisotropic diffusion filter to remove unwanted artifacts. After that, the contrast limited adaptive histogram equalization (CLAHE) is introduced to enhance the image contrast. Then the tumor is segmented using a multivariant thresholding and Chan-Vese algorithm. Now, the statistical features, texture features, wavelet features are measured to classify the segmented objects. Finally, the appropriate features are selected using a genetic algorithm and classify the segmented object using an artificial neural network. The performance of the proposed algorithm is tested on publicly available BRATS datasets. The experimental result showed that the proposed algorithm achieved 99.5% for the BRATS dataset and 98.3% for augmented BRATS dataset image of accuracy, which is better than many existing well known state-of-arts methods.

1. INTROUCTION:

Brain tumors are an unwanted cell growth without limitation [1-6]. Cancer is classified into malignant or benign in two forms. Benign tumors are homogenous organisms that do not contain cancer cells, whereas malignant tumors are carcinogenic. The American Brain Tumors Association [7] and the WHO have developed tumor grading systems, which have the name of benign grades I and II whereas grades III and IV are categorized as malignant. Grades I and II are categorized as benign. In contrast to malignant, benign growth is sluggish. The tumor is transformed into a high-grade tumor when low-grade tumors are not treated appropriately [8]. Therefore, the primary target for radiologists is brain tumor diagnosis [9]. Grade II gliomas patients require routine treatment and monitoring by means of MRI [10], since gliomas in clinical practice are more effective to confirm. Without any ionization radiation, the MRI gives a thorough human brain structure. This technique is considered ideal for the segmentation of brain tumors, but it is difficult to segment entirely and categorize healthy / abnormal images into a single MRI. Consequently, the MRI provides the capability to monitor multifactorial RMI sequences such as T1, T2, and T1c (DWI), which provide a comprehensive structure in the brain to accurately identify the tumor area [11]. The MRI is also known as MRI multimodality. MRI is useful in modeling and creating an abnormal brain atlas for the general pathological brain [12]. In segments of more than one RIM modality, the region-based and machine-learning techniques are employed [13].

The radiologist tests the tumor size, position and impact in the surrounding environment when a brain tumor is identified clinically. It is clear that tumor patients will substantially improve their chances of survival with correct tumor-range identification at the initial stage [14, 15]. Normal division methods are lacking when the tumor is near the location of the brain tumors [16] in cases of brain tumor. Existing work requires considerable improvement to increase tumor detection precision, applicability, and automation [17–20]. The moderate classification adaptive template [21] and the maximized expectation (EM) [22] are statistical methods that fail when many deformations occur in the brain area. Different MR images such as T2, T1 and enhanced contrast, PD and geometrical constraints are used to obtain final segmentation results to solve the problem [23]. For the study of tumor growth rates, the non-rigid deformation and fuzzy connectivity methods are used [24]. The fumigating approach is more sensitive to the noise requiring contact with the user [25]. Regional approaches are used to use local data from each voxel, but overall boundary and form constraints are not implemented. The semiautomatic technique, based on the level set where the user selects manually the tumor area, is proposed in contour-based methods. The results rely on visual inspection until the optimization of results [26]. For brain structure analysis, the deformable model and algorithm of neural networks are used [27].

There are many deep learning models available, but Conventional Neural Network (CNN) is commonly used in complicated operations with convolutional filters [28]. The CNN model includes sequences of feed forward layers of various filter sizes, bundles and fully linked layers that transform two-dimensional characteristics of

previous layers into a single-dimensional classification function vector [29]. CNN is one of the most popular building blocks for deep learning. CNN applications are commonly used by major corporations such as Google, Facebook, and Twitter because of its reputation. ELM is not commonly used in contrast to CNN, but it is also superior to profound learning methods in many current research ventures [30].

In this research work, has proposed a brain tumor detection algorithm that efficiently detects the brain tumor from the MRI image. In this paper, the introductory overview is described in section I. In section ll, it described the proposed method with required mathematical expression. The result and discussion are described in section lll and finally, end the paper with some concluding remarks.

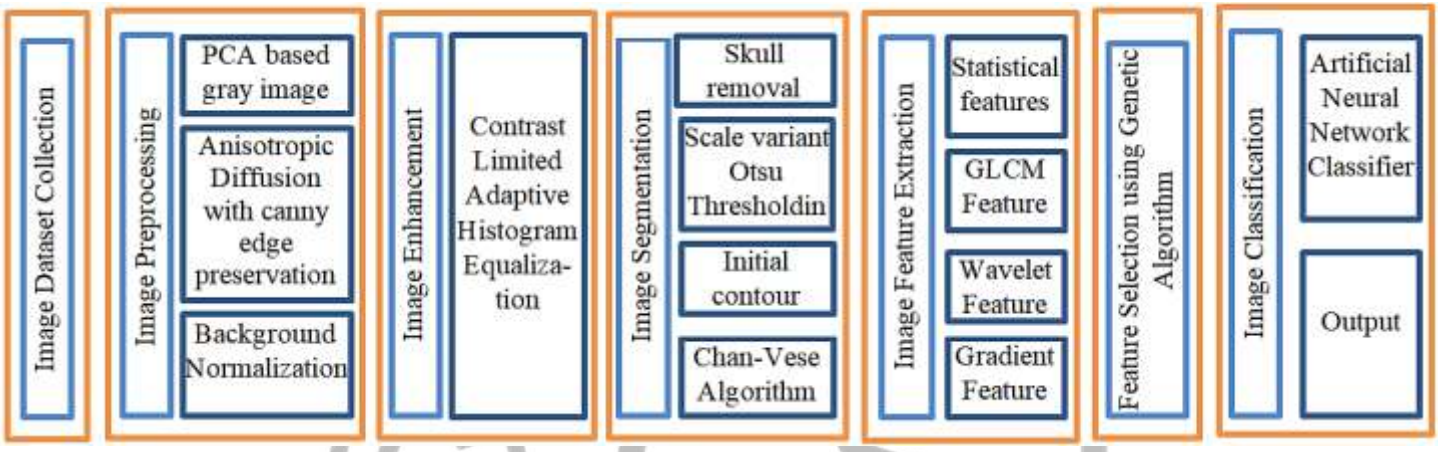

Fig. 1: Block diagram of the proposed brain tumor detection algorithm.

2. PROPOSED METHOLODGY

The early detection of brain tumors helps to decrease the mortality rate. The proposed brain tumor detection algorithm consist of image preprocessing, image enhancement, image segmentation, different types of features detection, feature selection and classification steps. The block diagram of the proposed algorithm is shown in Fig 1. The descriptions of the following steps are as below:

2.1 Input Image Collection

This section discusses the MRI image datasets. The proposed algorithm is texted on the BRATS [31] dataset image and the augmented image from 3D BRATS dataset [32]. The brain MRI image consists of a T1-weighted image with 1740 repetition time and 20 echo times. On the other hand, the T2 weighted MRI image generated with 130 echo time and 5850 repetition time. This MRI image is acquired from 3 Tesla siemens magneto spectra MR machine. There were 15 slices for each screen, leading to a total of 135 images per patient with 9 slices or images with 200 mm of the field of view, 1 mm of inter-slice spacing and 0.78 mm of voxel with 0.78 mm and 0.5 mm of diameter. In this proposed methodology used 512x512 MRI images.

2.2 Image preprocessing

The MRI image has low contrast and contained some unwanted artifacts. To remove the unwanted artifacts, the proposed algorithm has used Lab color pace transform coupled with principal component analysis (PCA). The Lab color space has a larger dimension than other color transformation and it is device-independent. The color representation in Lab related to human vision and does not any particular device output. The pixel intensity is

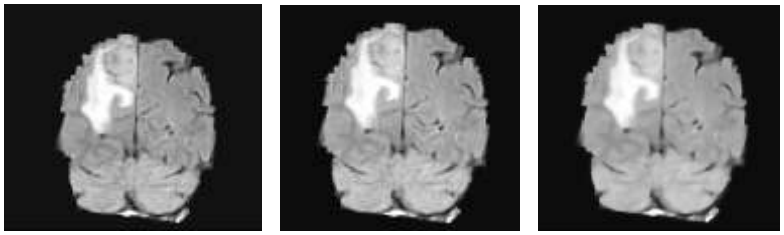

(a) (b) (c)

Fig. 2. Image preprocessing output, (a) Input MRI image, (b) PCA based gray scale image, (c) Noise removal using anisotropic difussion filter.

defined by the 'L' component, whose valu lies between block (0) and white (1). However, the 'a' component represents the color variation from green to red and similarly 'b' represents the color variation from blue to yellow. The PCA has low noise sensitivity and has reduced image grouping complexity. The PCA is used to visualize the multilevel inter-correlated data. However, it helps to identify the direction of intensity variation. To remove the unwanted artifacts the Gaussian filter is widely used. The Gaussian averaging filter removes the salt and pepper noise, while the edge information also removed. Finally, the anisotropic diffusion output and the edge pixel are added to generate the noise-free edge preserved MRI output. The diffusive process has been formulated in [33] to remove the noise. The diffusion process is iterative and the mathematical formulation can be formulated as follows:

$$\frac{\partial}{\partial t}\mu(x,y,\rho) = div\left(\phi(x,y,\rho)\nabla\mu(x,y,\rho)\right) \tag{1}$$

The strength of the diffusion is controlled using $\phi(x,y,\rho)$. The order of the process is represented by ρ and the variable x and y represent the spatial coordinates. The image intensity I(x,y,t) is represented by the function $\mu(x,y,\rho)$. The diffusion function $c(x,y,\rho)$ directly dependson the gradient of $I(x,y,\rho)$. The $\phi(x,y,\rho)$ is a monotonically decreasing function, which diffuse within the region and does not affect region boundaries of a higher gradient. The diffusion function can be expressed as

$$\phi(x,y,\rho) = f\left(\left|\nabla I(x,y,\rho)\right|\right) \tag{2}$$

The noise removal image is normalized using equation 3 as

$$I_{nom} = \frac{I_{rn} - \min(I_{rn})}{\max(I_{rn}) - \min(I_{rn})}(\mathrm{L}-1) \tag{3}$$

The image preprocessing output is shown in Fig. 2., the first image is the input MRI image which is converted into the grayscale image as shown in Fig. 2 (b). The noise removal image is shown in Fig. 2 (c).

2.3 Contrst Enhancement

The contrast limited adaptive histogram equalization (CLAHE) has great success to enhance the medical image efficiently, it is one of the widely used low contrast medical image enhancement algorithm. The MRI image is divided into nxn image sub-block and measure the histogram of each image block. Then, set the clipping limit as a threshold of each sub-block [34]. The higher value of clipping limits increases the contrast of the local image subblock. However, the histogram is transformed in such a way that, it doesn't exceed the clipping limit. The mathematical expression of uniform distribution given as

$$\chi = \left[\chi_{\max} - \chi_{\min}\right] * p(f) + \chi_{\min} \tag{4}$$

Here p(*f*) is the cumulative probability distribution (CPD). χ is the computed pixel value. The exponential distribution can be adapted as

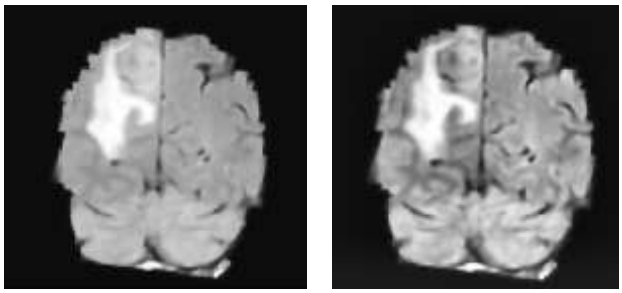

(a) (b)

Fig. 3. Contrast enhanced output, (a) Input denoisy image, (b) Respective contrast enhanced output.

$$\chi = \chi_{\min} - \left(\frac{1}{a}\right) * \ln\left[1 - p(f)\right] \tag{5}$$

The CDF followed the Rayleigh distribution as

$$CDF = p\left(f\left(x/b\right)\right) = \int_0^x \frac{x}{b^2} e^{\frac{-x^2}{2b^2}} \tag{6}$$

The neighboring subblocks were combined using bilinear interpolation and the image histogram is altered according to the modified histogram. The contrast enhanced image is shown in Fig. 3.

2.4 Segmentation

The segmentation of the tumor from the MRI image consists of skull removal, multi-level thresholding based object detection, and application of the Chan-Vese algorithm. At first, the Otsu thresholding algorithm is applied to calculate the threshold of the enhanced MRI image and converted it into a binary image. Then fill the binary objects, this fills binary image xor with the original binary image. The xor image is the representation of the skull removal image. Now, again calculate the threshold using the Otsu method [35], and using this threshold convert the skull removal image into a binary image. Again set another threshold which is less than the previous threshold, using this threshold convert the binary image. Now, add these two binary images and combine all detected object into one object. In this proposed algorithm, the above process is repeated three times. This process repeated to detect all possible tumor regions. The detected objects are dilated to increase the detected ob-jects region. These objects are set as the initial contour of the Chan-Vese algorithm. Now, apply the Chan-Vese algorithm to detect the final segmented objects. Chan-Vese is an active contour model use Munford-Shah function [36] for segmentation. This model minimizes the energy, which reformulates level set and solves the energy minimization problem. The energy minimization function is defined as:

$$F\left(c_1, c_2, C\right) = \mu.Length\left(C\right) + \nu.\mathrm{Area}\left(inside\left(C\right)\right) + \lambda_1 \int_{inside(C)} \left|u_0\left(x,y\right) - c_1\right|^2 dxdy + \lambda_2 \int_{outside(\mathrm{C})} \left|u_0\left(x,y\right) - c_2\right|^2 dxdy \tag{7}$$

Where, $\mu \geq 0$, $V \geq 0$, $\lambda_1, \lambda_2 > 0$. If β be a bounded open set of $\mathbb{R}^2$and u_0 be the imput image than C represent the curve. If $C \subset \beta$ than the level set method can be described using Lipschitz function $\Phi: \beta \rightarrow \mathbb{R}$, so that

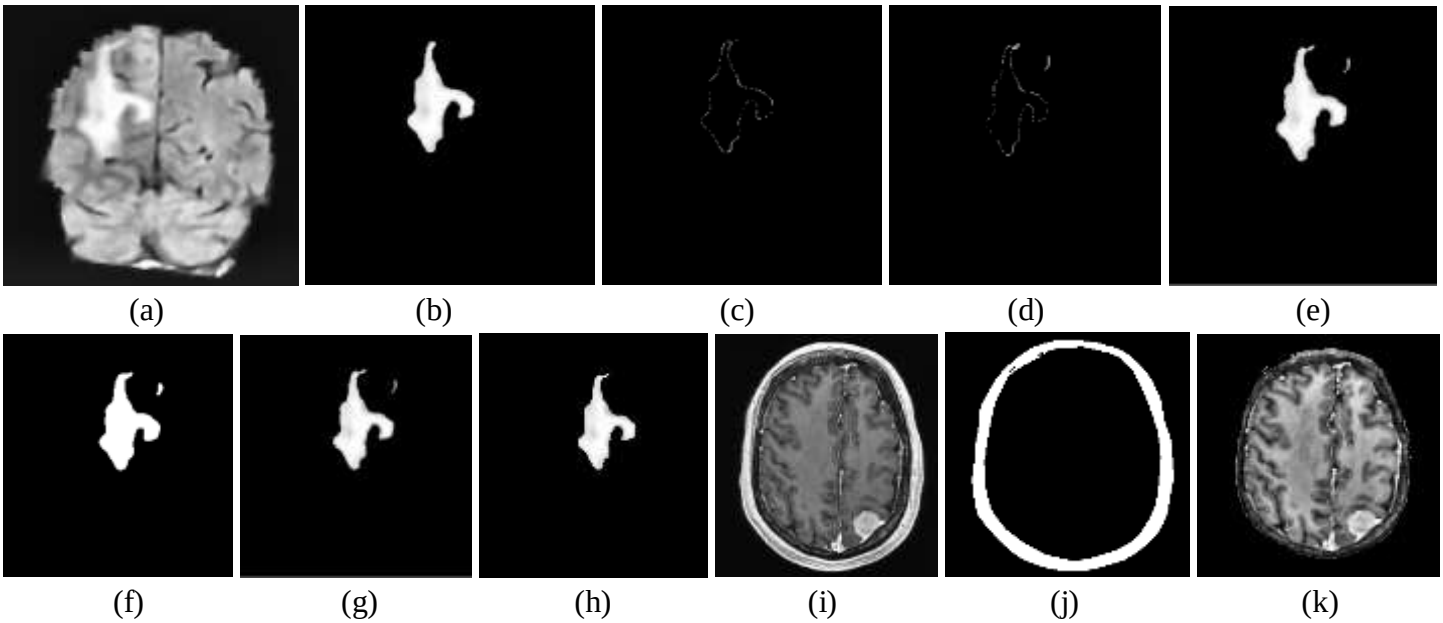

Fig. 4. Tumor segmentation output, (a) Input contrast enhanced Mri image, (b) output by applying initial threshold (c) 2nd segmented output, (d) 3rd segmented output, (e) Combine all segmented output, (f) Initial tnotour, (g)Output of Chan-Vese algorithm, (h) Final segmented tumor, (i) Input MRI image contain skull, (j) segmented skull, (k) Skull removal MRI image.

$$\begin{cases} C = \partial\psi = \{(x,y) \in \beta : \Phi(x,y) = 0\} \\ inside(C) = \psi = \{(x,y) \in \beta : \Phi(x,y) > 0\} \\ outside(C) = \beta \setminus \bar{\psi} = \{(x,y) \in \beta : \Phi(x,y) < 0\} \end{cases} \tag{8}$$

For a given contour C the $\Phi(x,y)$ is the sign function, which is positive insithe the contour C and negative outside the contour C. The segmentation process with output is shown in Fig. 4. The first image is the enhanced image; image 4(b) to 4(e) is the step by step threshold based segmentation. Fig 4(f) is the initial contour, which is applied in the Chan-Vese algorithm. The Fig 4(g) is the output of the Chan-Vese algorithm and the segmented large object is shown in Fig 4(h). The skull removal output is represented by Fig 4(i) to 4(k). Fig. 4(i) is the input image that have skull and the Fig 4(j) is the segmented skull. The function $F(c_1,c_2,C)$ can be representedin terms of $\Phi(x,y)$ as

$$F(c_1,c_2,\Phi) = \mu \int_\beta \delta_0(\Phi(x,y)) |\nabla\Phi(x,y)| dxdy + \nu \int_\beta H(\Phi(x,y)) + \lambda_1 \int_\beta |u_0(x,y) - c_1|^2 H(\Phi(x,y)) dxdy + \lambda_2 \int_\beta |u_0(x,y) - c_2|^2 H(1 - \Phi(x,y)) dxdy \tag{9}$$

Where, $Length(\mathrm{C}) = \int_{\beta} \left|\nabla H\left(\Phi(\mathrm{x},\mathrm{y})\right)\right| dxdy = \int_{\beta} \delta_0(\Phi(\mathrm{x},\mathrm{y}))\left|\nabla\Phi(\mathrm{x},\mathrm{y})\right| dxdy$

$$H(\mathrm{z}) = \begin{cases} 1, & if \quad z \geq 0 \\ 0, & if \quad z < 0 \end{cases} \tag{10}$$

$$Area(\mathrm{inside(C)}) = \int_{\beta} H(\Phi(\mathrm{x},\mathrm{y}))\,\mathrm{dxdy} \tag{11}$$

2.5 Feature Extraction

The features are Autocorrelation, Contrast, Correlation, Cluster Prominence, Cluster Shade, Dissimilarity, Energy, Entropy, Homogeneity, Maximum probability, Variance, Sum average, Sum variance, Sum entropy, Difference variance, Difference entropy, Information measure of correla-tion, Angular Second Moment, Inverse difference is homom, Inverse difference normalized, Inverse difference moment normalized. The image statistical information can be expressed by the image histogram. For any gray scale image I(x,y) having intensity level 0,1…,N-1, then the probability and histogram of each intensity expressed as

$$p(\mathrm{i}) = \frac{h(\mathrm{i})}{nm} \qquad for\, i = 0,1,2 \ldots N-1 \tag{12}$$

$$h(\mathrm{i}) = \sum_{x=1}^{n}\sum_{y=1}^{m} \psi(\mathrm{I(x,y),i}) \tag{13}$$

Here ψ(i,j) are the Kronecker delta function that can be written as

$$\psi(\mathrm{i,j}) = \begin{cases} 1, & i = j \\ 0, & i \neq j \end{cases} \tag{14}$$

To calculate the statistical parameter the mentioned parameter are used as bellows.
Mean: it represent the average intensity value.

$$\mu = \sum_{i=0}^{n-1} i.\mathrm{p(i)} \tag{15}$$

Variance: it measures the variation around the mean value.

$$\sigma^2 = \sum_{i=0}^{n-1} (i-\mu)^2\, p(i) \tag{16}$$

Skewness: it represents the symmetry around the mean.

$$\mu_3 = \sigma^{-3} \sum_{i=0}^{n-1} (i-\mu)^3\, p(\mathrm{i}) \tag{17}$$

Kurtosis: it measure the fitness in the histogram

$$\mu_4 = \sigma^{-4} \sum_{i=0}^{n-1} (i-\mu)^4\, p(\mathrm{i}) - 3 \tag{18}$$

Entropy: measure the uniformity of the histogram

$$H = \sum_{i=0}^{n-1} p(\mathrm{i}) \log_2 [\, p(\mathrm{i})] \tag{19}$$

Energy: represents the mean square of each pixel intensity

$$E = \sum_{i=0}^{n-1} [\, p(\mathrm{i})]^2 \tag{20}$$

The above parameters are used to calculate the texture feature. The gray level co-occurrence matrix (GLCM) represents the probability distribution of each pixel. The total neighboring pixels R(d,θ) is used to divide the image matrix, which represent the joint probability $P_{d,\theta}(x,y)$ of two pixels with distance d. where d=1,2…. and $\theta=0^0$, 45^0, 90^0, 135^0. The GLCM features are as follows

Angular Second Moment (ASM): represent uniformity

$$ASM = \sum_{x=1}^{n-1} \sum_{y=1}^{m-1} [\, p(x,y)]^2 \tag{21}$$

$$Contrast = \sum_{\mathrm{x,y}=0}^{n-1} p_{ij} \left(x-y\right)^2 \tag{22}$$

$$Absolute \quad Value = \sum_{x=0}^{n-1} \sum_{y=0}^{m-1} |x-y|\, p(ix,y) \tag{23}$$

$$Inverse \quad Difference = \sum_{x=0}^{n-1} \sum_{y=0}^{m-1} \frac{p(x,y)}{1+(x-y)^2} \tag{24}$$

$$Entropy = -\sum_{x=0}^{n-1} \sum_{y=0}^{m-1} p(x,y) \log_2 [\, p(x,y)] \tag{25}$$

$$\mathrm{Homogeneity} = \sum_{x,y=0}^{n-1} \frac{p_{xy}}{1+(\mathrm{x}-y)^2} \tag{26}$$

$$Correlation = \sum_{x,y=0}^{n-1} p_{x,y} \frac{(\mathrm{x}-\mu)(\mathrm{y}-\mu)}{\sigma^2} \tag{27}$$

$$Shade = sign(\mathrm{A})|A|^{1/3}, \qquad A = \sum_{x,y=0}^{n-1} \frac{(\mathrm{x}+y-2\mu)^3\, p_{xy}}{\sigma^3(\sqrt{2(1+C)})^3} \tag{28}$$

$$pro\min ence = sign(\mathrm{B})|B|^{1/4}, \qquad B = \sum_{x,y=0}^{n-1} \frac{(\mathrm{x}+y-2\mu)^4\, p_{xy}}{4\sigma^3(1+\mathrm{C})^2} \tag{28}$$

The segmented possible tumor is converted into the frequency domain by applying the CDF9/7 wavelet transform [37]. The wavelet coefficients represent both the spatial and frequency resolution. However, the single level wavelet transforms separate the image into low, low-high, high-low and high-frequency block. Now, calculate the Contrast Correlation, Energy, Homogeneity, Mean, Standard_Deviation, Entropy, RMS, Variance, Smoothness, Kurtosis, Skewness, Inverse difference moment. The mathematical expression is similar as mention above.

2.6 Feature Selection

A genetic algorithm (GA) is a population-based optimization algorithm. A genetic algorithm is a heuristic search inspired by the theory of the natural evolution of Charles Darwin. The algorithm illustrates the selection process in which the fittest individuals are selected for reproduction to produce the offspring of the next

generation [38-41]. The natural selection process starts with the selection of the best individuals from a population. They produce descendants which inherit parents ' characteristics and are added to the next generation. When parents have better fitness, they would have a better offspring than parents and a higher chance of survival. The process continues to iterate and in the end, a generation of the most suitable individuals is identified. In a GA one set of chromosomes (solution candidates) manipulate to create a new set by genetic functional steps including a mutation and a crossover. The state of solution candidates (chromosomes) is evaluated with a function generally known as objective or fitness test. In other words, fitness (target function) generates numerical values that are used in the population ranking of chromosomes. The fitness function is formulated base on which problem is resolved. The parabolic is a perfect example of a fitness function. The GA deals with binary search space because the chromosomes are bit chains. In the nature of human natural evolution, GA manipulates the finite binary population. First of all, an initial population (mostly randomly) is generated and assessed using a fitness function. The gene value ' 1 ' indicates that the unique feature indexed by the ' 1 ' location is selected for the binary chromosome used, otherwise (i.e. ' 0 '), the chromosomal evaluation function is not selected. The GA based feature selection process is presented in Fig. 5. At first, initialize the population size x with chromosome having the binary random digits. The population size indicates the number of chromosomes and the length of the chromosome indicate the number of bits in each chromosome. The initial population is chosen randomly. The feature subsets are selected by evaluating the discriminative capacity. In this proposed algorithm the fitness of each chromosome is evaluated by using K-nearest neighbor (KNN). The kNN algorithm has solved the classification problem by finding the shortest path between training and testing data. To find the shortest path, the KNN algorithm finds the Euclidean distance between training and testing data sets. The fitting process is mathematically represented by the following expression.

$$fit = \frac{\alpha}{v_f} + e^{\left(\frac{-1}{v_f}\right)} \tag{29}$$

Here, Vf is selected feature, α ids the error of the KNN classifier.

The new population is generated by using the crossover and mutation operation (Elitism and Genetic operators) and creates three types of children from each new population [42]. The Elite children are those children, who have the best chromosomes and push them into the next generation automatically. The two best-fit chromosomes are considering Elite children. The fractions of the next generation kids, which are created by the crossover operation, are called crossover children. In this work, the cross over fraction 0.7 is used. The rest of the features are considered the mutation of children. The GA use selection mechanism to ensure that, the candidate's solutions are constantly improves over each fitness value. In this work, use the stochastic uniform method with size 4. Two functions are used in tournament selection to make sure that the worst feature does not propagate into the next steps. The parents are generated in one function and the other function finding the winner of the tournament and ranked all chromosomes according to the fitness score. The best of these is the winner and the first two are considered the Elite children. The tournament selection process is iterative and the GA continued to evaluate until the new population is filled up. The overall process is repeated until the GA reaches onto the optimal solution.

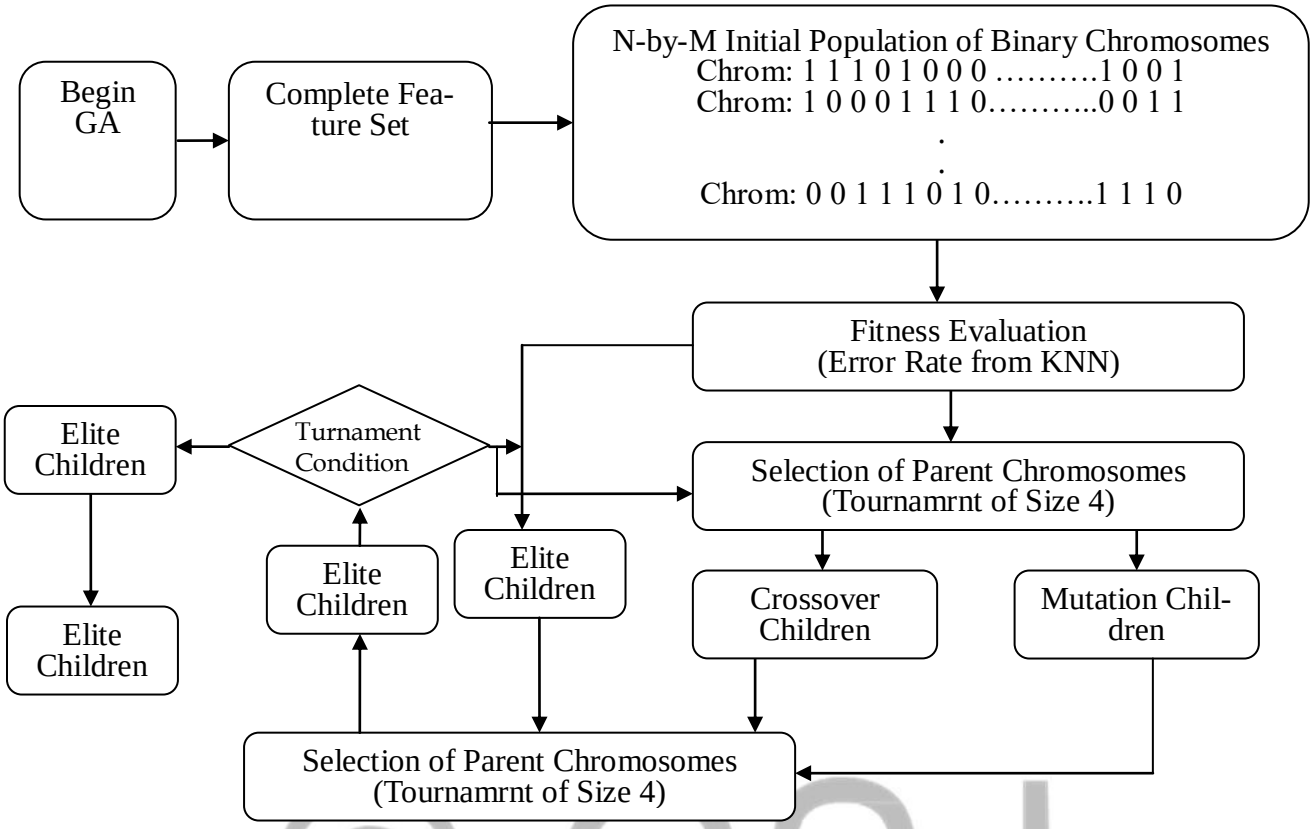

Fig 5: Ganetic Algorithm based feature selection

2.7 Classification

Artificial Neural Networks (ANN) are capable of learning and modeling non-linear and complex relationships, which are important since many of the relations between inputs and outputs in real life are both non-linear and complex. In the proposed algorithm has used ANN as a classifier, which is used to classify the segmented objects. The feature is taken from the feature selection section and train the neural network using the selected features. This algorithm introduced a feed-forward artificial neural network (ANN) with a backpropagation algorithm. The error is calculated using a gradient descent algorithm and the error is fed back into the network to update the weight of the network. The initial weight and bias values are set randomly with small values. These weights, biases and inputs are used to measure the outputs of NN. In this proposed algorithm use three layers ANN (input, hidden and output layer). The number of neurons used in the hidden is 60 and uses ReLu activation function in the hidden layer. However, the output layer has one neuron and used the sigmoid activation function.

3. Result and Discussion

To examine the performance of the proposed brain tumor detection model used the BRATS dataset [32]. Which consist of 217 MRI image and all images have different modalities like FLAIR T1 and T2. Among the 217 images, 187 images contain tumor and 30 MRI images contains no tumor. On the other hand, another dataset of 699 images is generated from the 3D BRATS image. For training the dataset, the total image is split into training, testing, and validation. The performance of the proposed algorithm is expressed with accuracy. The accuracy

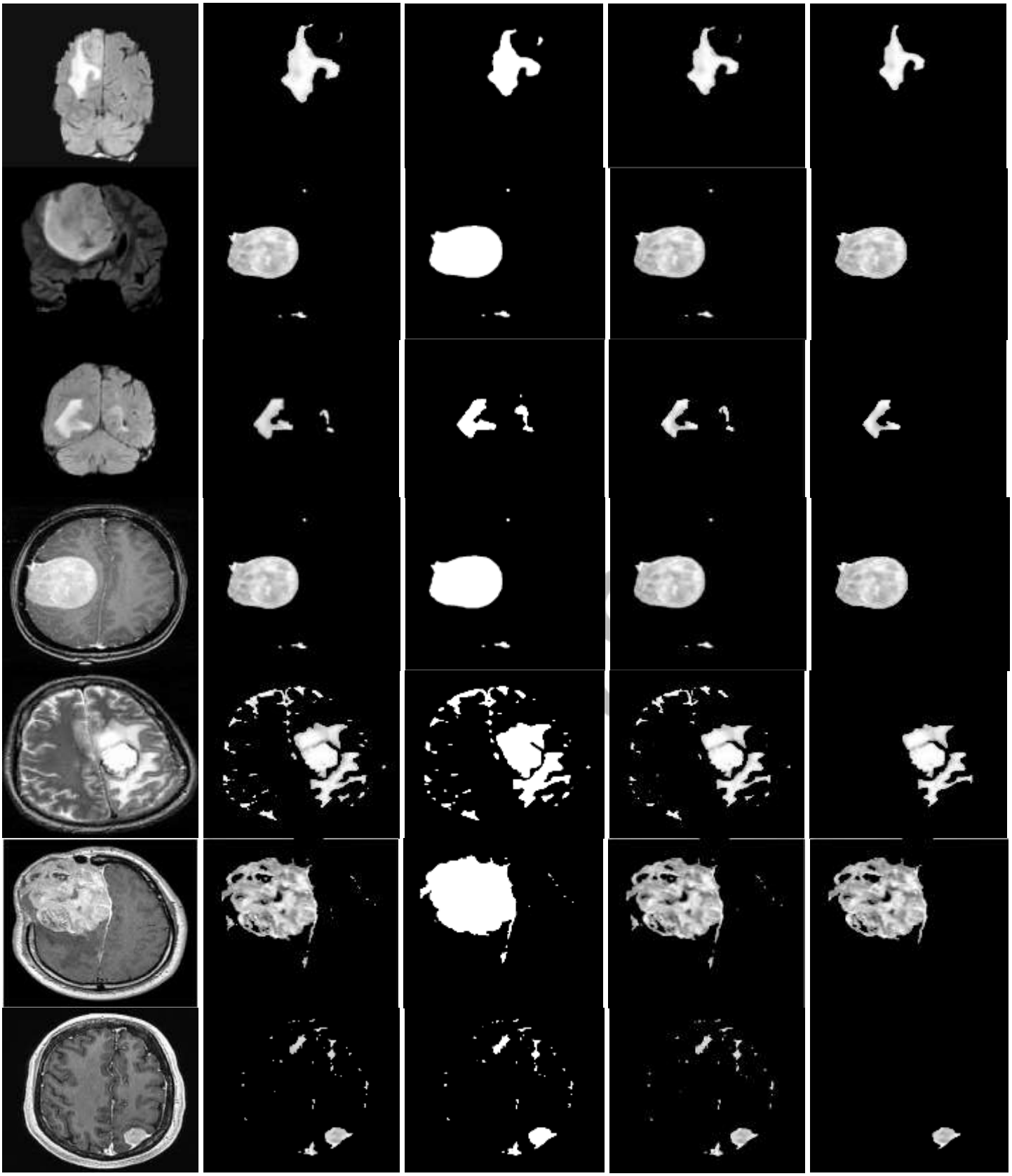

(a) (b) (c) (d) (e)

Fig. 6. Steps by step output of the proposed algorithm, (a) Input MRI image, (b) Primary segmentation, (c) Initial Countor, (d) Output of Chan-Vese algorithm, (e) Final segmented output.

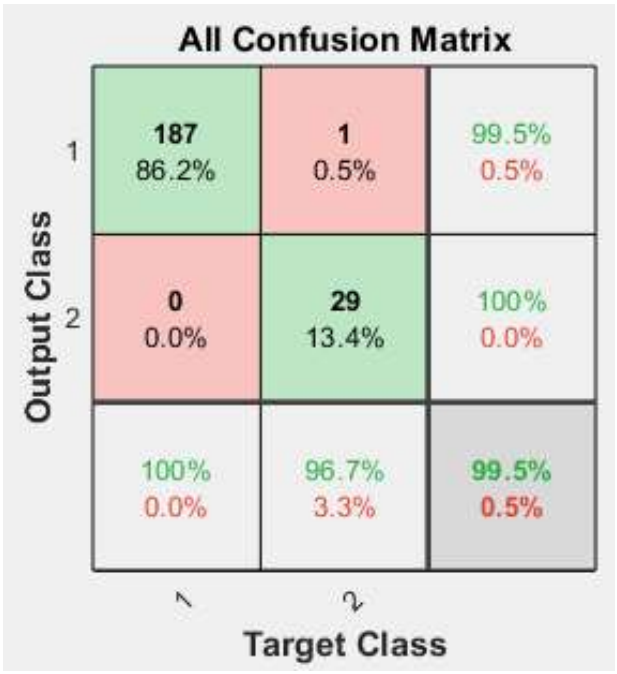

(a)

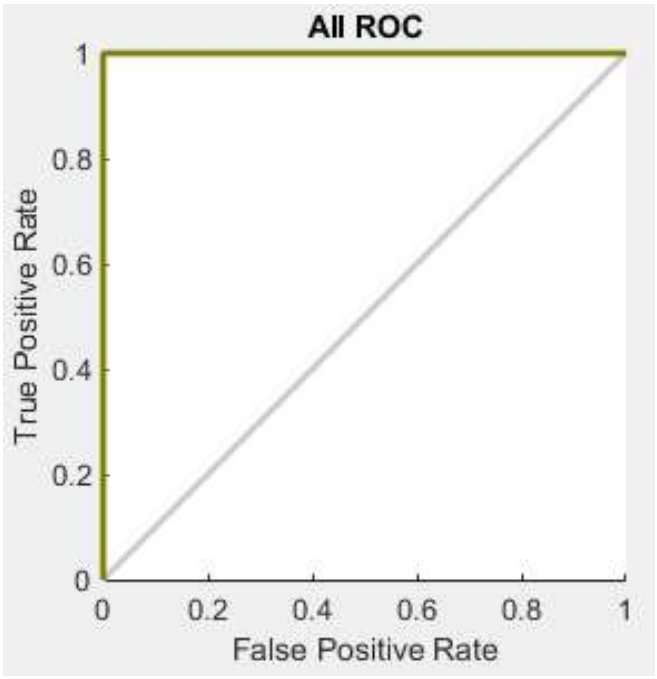

(b)

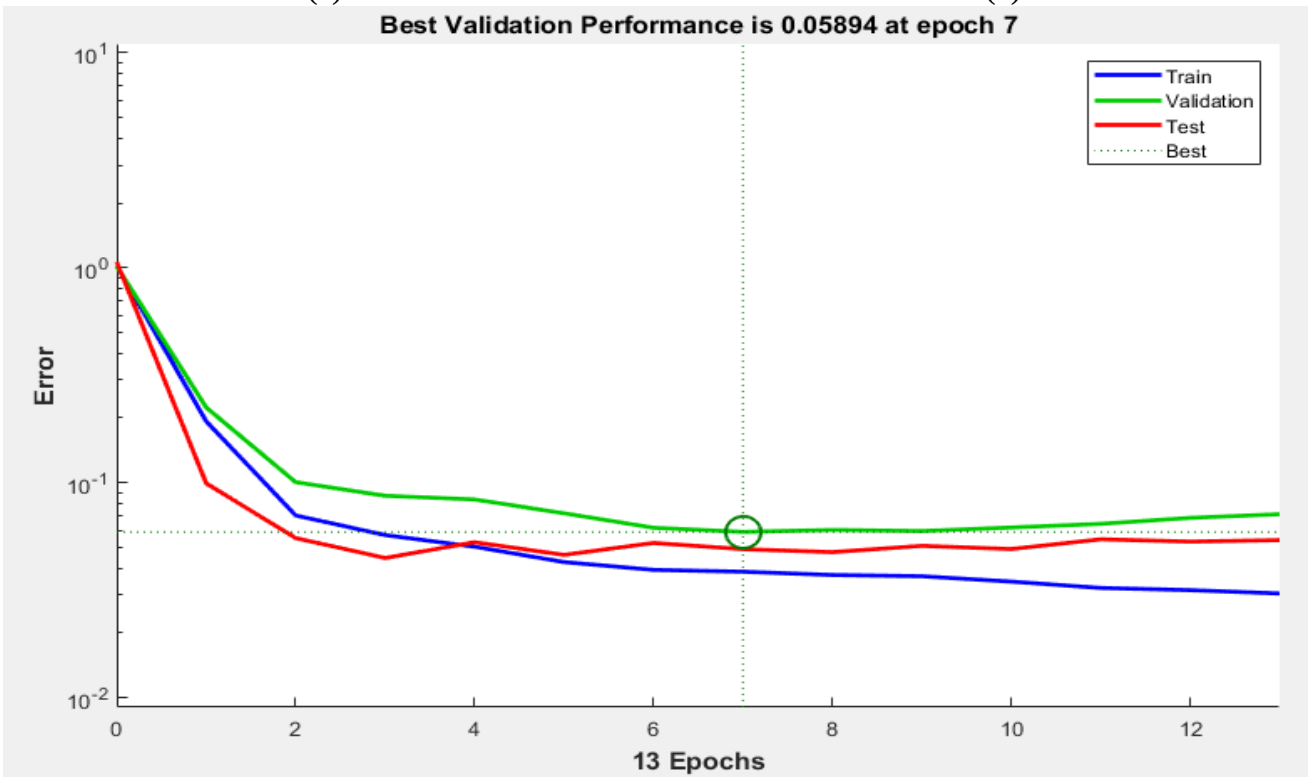

(c)

Fig. 7. performances of the trained network, (a) Confussion matrix, (b) respective ROC output and (c) training performances.

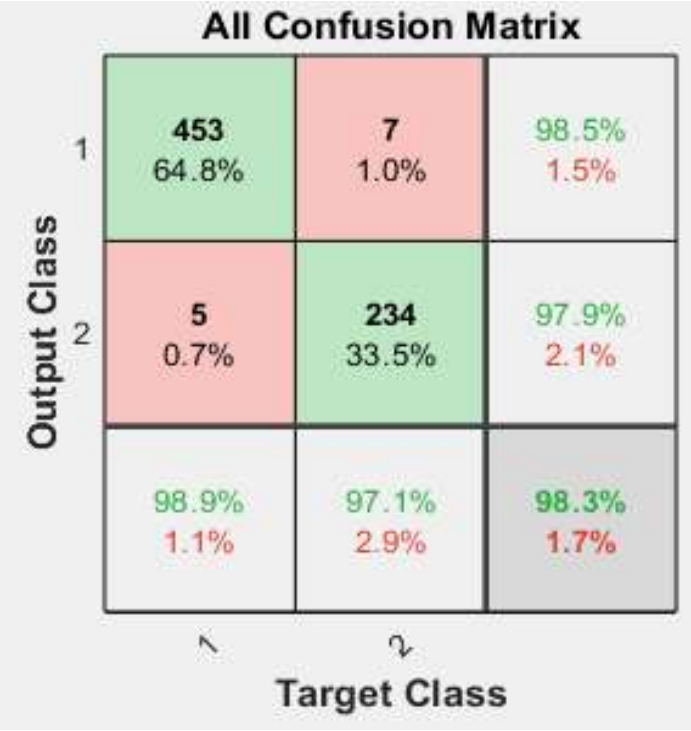

(a)

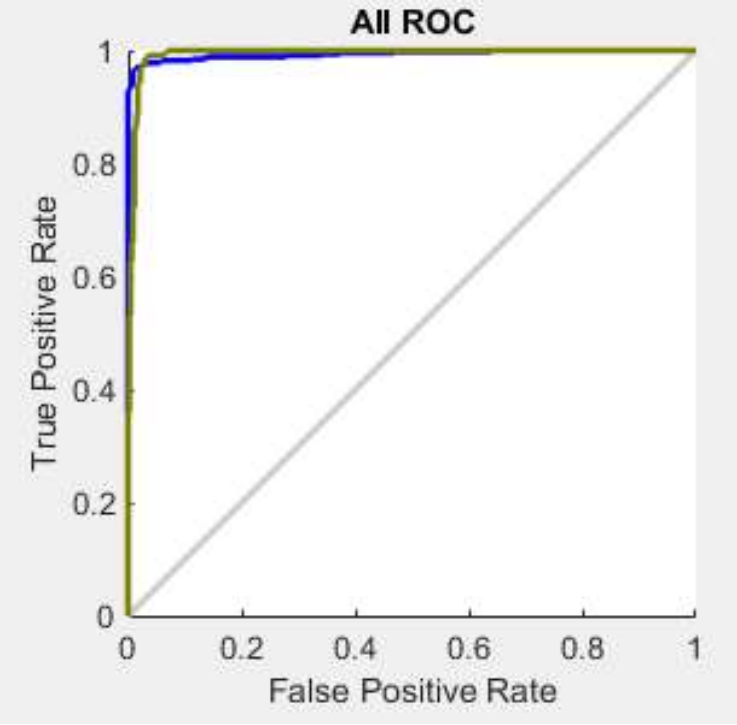

(b)

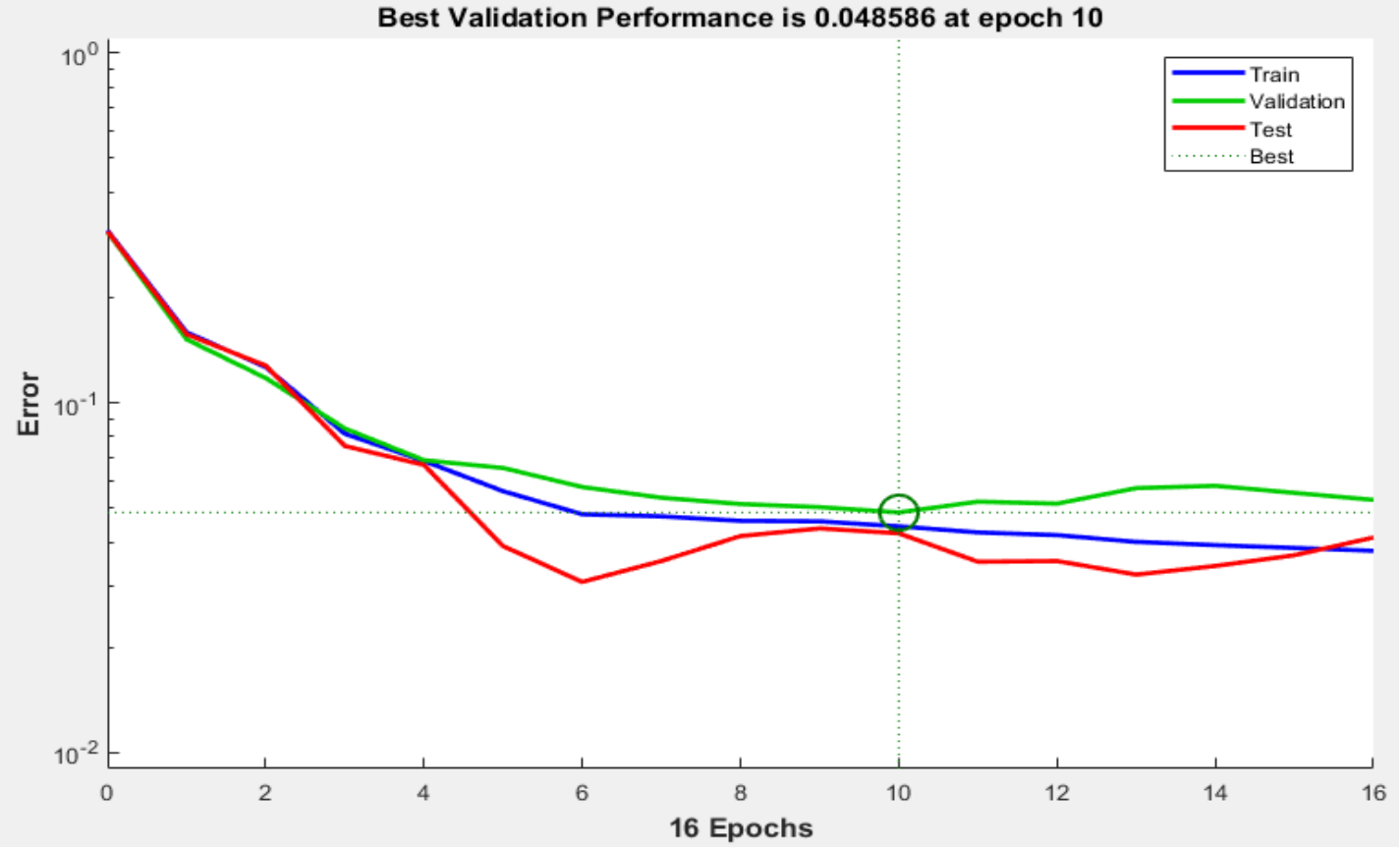

(c)

Fig. 8. Performances of the trained network, (a) Confussion matrix, (b) respective ROC output and (c) training performances.

is proportional to the amount of correct tumor detection. The input MRI image is preprocessed, enhanced, segment, feature extraction, feature selection and classification, which is described in the methodology section. The step by step output of the proposed algorithm is shown in Fig. 6. The first column of Fig.6 is the input MRI image, the first three images are taken from a created dataset and the other four are taken from the BRATS dataset. The tumor segmentation using multi-valued thresholding is shown in Fig. 6 (b). The initial contour of the Chan-Vese algorithm is shown in Fig. 6 (d). However, the output of the Chan-Vese algorithm and the final tumor are shown in Fig. 6 (e) and Fig. 6 (f). The feature extraction is done from the segmented objects. Two types of features are extracted, twenty-one statistical features, and thirteen wavelet features. The statistical features of seven images (as shown in Fig 6 (a)) are listed in Table 1 and Table 2 represent the texture and wavelet feature respectively. The twenty one features are Autocorrelation (Auto), Contrast (Cont), Correlation (Corr), Cluster Prominence (ClustP), Cluster Shade (ClustS), Dissimilarity (DisSim), Energy (Ener), Entropy (Entr), Homogeneity (Homo), Maximum probability (MaxP), Variance (Vari), Sum average (SumA), Sum variance (SumV), Sum entropy (SumE), Difference variance (Dvari), Difference entropy (Denrt), Information measure of correlation (InCo), Angular Second Moment (ASM), Inverse difference is homom (IDH), Inverse difference normalized (IDN), Inverse difference moment normalized (IDMN). The texture features are Contrast Correlation, Energy, Homogeneity, Mean, Standard_Deviation, Entropy, RMS, Variance, Smoothness, Kurtosis, Skewness, Inverse difference moment (IDM). The 34 feature is applied to the genetic algorithm to select significant features. Among the 48 feature, the GA select 25 significant feature, which is used to train the proposed neural network. The training performance, confusion matrix and the receiver operating characteristic curve (ROC) are shown in Fig. 7 and Fig. 8. Fig. 7 is the representation for BRATS image and Fig. 8 is the training and performance representation of created dataset from 3D BRATS. The comparison of the accuracy of the proposed algorithm with the existing algorithm has shown in Table 3. The comparison result has shown that the proposed algorithm provides better accuracy (99.5% for BRATS dataset and 98.3% for the created dataset from 3D BRATS datasets) than [44-49] and comparable with 99.81% [43].

Table 1: Statistical features of the segmented objects.

Img	Auto	Cont	Corre	ClustP	ClustSha	DisSim	Ener	Entr	Homo	MaxP	Vari	SumA	SumV	SumE	Dvari	Dentr	InCo	ASM	IDH	IDN	IDMN
(a)	2.493	0.199	0.917	749.299	57.157	0.036	0.941	0.185	0.993	0.993	0.970	2.555	2.367	9.357	0.178	0.199	0.065	-0.739	0.441	0.997	0.719
(b)	5.315	0.125	0.977	912.053	89.926	0.053	0.759	0.701	0.980	0.979	0.870	5.327	3.232	17.527	0.666	0.125	0.179	-0.789	0.774	0.995	0.884
(c)	1.951	0.103	0.931	447.521	35.254	0.022	0.959	0.143	0.995	0.995	0.979	1.968	2.240	7.311	0.138	0.103	0.052	-0.749	0.397	0.998	0.698
(d)	5.166	0.106	0.982	1283.820	113.385	0.035	0.826	0.473	0.988	0.988	0.908	5.171	3.060	18.181	0.457	0.106	0.116	-0.818	0.693	0.997	0.845
(e)	5.008	0.262	0.955	1614.563	129.221	0.057	0.851	0.411	0.987	0.986	0.921	5.093	2.967	18.104	0.395	0.262	0.122	-0.773	0.636	0.995	0.816
(f)	11.869	1.437	0.885	758.108	132.288	0.356	0.489	1.490	0.909	0.902	0.694	12.577	5.032	37.303	1.329	1.437	0.612	-0.529	0.812	0.969	0.891
(g)	2.267	0.626	0.712	402.604	36.167	0.156	0.864	0.484	0.964	0.959	0.930	2.542	2.444	7.802	0.424	0.626	0.293	-0.352	0.432	0.987	0.709

Table 2: Wavelet features of the segmented objects.

Img	Cont	Corr	Ener	Homo	Mean	StandD	Entr	RMS	Vari	Smooth	Kust	Skew	IDM
(a)	0.241	0.164	0.900	0.971	0.003	0.071	0.927	0.071	0.005	0.989	52.091	3.649	5.152
(b)	0.243	0.079	0.886	0.969	0.003	0.071	1.588	0.071	0.005	0.987	56.954	3.908	33.589
(c)	0.320	0.094	0.925	0.977	0.004	0.071	0.805	0.071	0.005	0.991	97.549	6.955	3.414
(d)	0.044	0.992	0.829	0.994	0.072	0.229	1.010	0.143	0.043	1.000	9.729	2.931	53.133
(e)	0.238	0.101	0.884	0.968	0.003	0.071	1.455	0.071	0.005	0.990	53.284	3.783	0.538
(f)	0.126	0.091	0.841	0.958	0.002	0.071	3.217	0.071	0.005	0.987	10.901	0.747	3.431
(g)	0.145	0.088	0.850	0.960	0.002	0.071	2.820	0.071	0.005	0.988	21.097	1.440	1.566

Table 3: Accuracy comparison of the proposed algorithm with existing methods.

Year	Reference	Method	Accuracy (%)
2020	Nasor et. al. [43]	Patch Processing, k-means Clustering and Object Counting	0.9981
2018	Gujar et. al. [44]	Genetic Algorithm	0.8967
2018	Kullayamma et. al. [45]	Convolutional Neural Networks	0.9262
2013	Attya et. al. [46]	GLCM and k-nearest neighbor (K-NN)	88.0
2013	Ibrahim et. al. [47]	ANN Back Propagation	96.33
2020	Gumaste et. al. [48]	Advanced Textural Feature Extraction	92.60
2020	Bandyopadhyay et. al. [49]	Texture Feature, Fuzzy Classifier	96.66
	Proposed method	Txture, stastital, and wavelet Feature, GA, ANN	99.5 () 98.3 ()

4. Conclusion

The brain tumor segmentation is a multiclass classification problem. In this paper, I proposed a brain tumor detection and classification algorithm that efficiently detect the brain tumor from the input MRI image and classify whether the input MRI image contains a tumor or not (for 217 BRATS image) and benign or malignant for the created dataset from 3D BRATS image. The proposed algorithm consists of image preprocessing, image enhancement, image segmentation using multi-valued threshold and Chan-Vese algorithm, feature extraction, feature selection, and classification. The proposed algorithm is tested on well-known BRATS datasets and augment-ed dataset. The experimental result provides above 98 percent accuracy, which is better than many existing algorithms. The segmentation and classification using deep learning can improve the multiscale classification more efficiently, which can be incorporated in future.

References

[1] Zhao L, Jia K, 'Deep feature learning with discrimination mechanism for brain tumor segmentation and diagnosis', International conference on intelligent information hiding and multimedia signal processing (IIH-MSP). IEEE, pp 306–309, 2015.

[2] Moise D, Madhusoodanan S, 'Psychiatric symptoms associated with brain tumors: a clinical enigma'. CNS Spectr 11(1):28–31, 2006.
[3] Morrison J, 'When psychological problems mask medical disorders: a guide for psychotherapists'. Guilford Publications, New York, 2015
[4] Sharif M, Tanvir U, Munir EU, Khan MA, Yasmin M, 'Brain tumor segmentation and classification by improved binomial thresholding and multi-features selection', J Ambient Intell Humaniz Comput 1–20, 2018.
[5] Amin J, Sharif M, Yasmin M, Fernandes SL, 'A distinctive approach in brain tumor detection and classification using MRI'. Pattern Recognit Lett 1–10, 2017.
[6] Amin J, Sharif M, Raza M, Yasmin M, 'Detection of brain tumor based on features fusion and machine learning'. J Ambient Intell Humaniz Comput 1–17, 2018.
[7] DeAngelis LM, 'Brain tumors'. New Engl J Med 344(2):114–123, 2001.
[8] Kleihues P, Burger PC, Scheithauer BW, 'The new WHO classification of brain tumours'. Brain Pathol 3(3):255–268, 1993.
[9] Naik J, Patel S, 'Tumor detection and classification using decision tree in brain MRI'. Int J Comput Sci Netw Sec (IJCSNS) 14(6):87, 2014.
[10] American Brain Tumor Association (ABTA). www.abta.org, accessed 2 January 2020.
[11] Abbasi S, Tajeripour F, 'Detection of brain tumor in 3D MRI images using local binary patterns and histogram orientation gradient'. Neurocomputing 219:526–535, 2017.
[12] Gordillo N, Montseny E, Sobrevilla P, 'State of the art survey on MRI brain tumor segmentation'. Magn Reson Imaging 31(8):1426–1438, 2013.
[13] Menze BH, Jakab A, Bauer S, Kalpathy-Cramer J, Farahani K, Kirby J, Burren Y, Porz N, Slotboom J, Wiest R (2015) The multimodal brain tumor image segmentation benchmark (BRATS). IEEE Trans Med Imaging 34(10):1993–2024
[14] Liu J, Li M, Wang J, Wu F, Liu T, Pan Y (2014) A survey of MRI-based brain tumor segmentation methods. Tsinghua Sci Technol 19(6):578–595.
[15] Coatrieux G, Huang H, Shu H, Luo L, Roux C (2013) A watermarking-based medical image integrity control system and an image moment signature for tampering characterization. IEEE J Biomed Health Inform 17(6):1057–1067
[16] Xie K, Yang J, Zhang Z, Zhu Y (2005) Semi-automated brain tumor and edema segmentation using MRI. Eur J Radiol 56(1):12–19
[17] Naz I, Muhammad N, Yasmin M, Sharif M, Shah JH, Fernandes SL (2019) Robust discrimination of leukocytes protuberant types for early diagnosis of leukemia. J Mech Med Biol 19:1950055
[18] Rajinikanth V, Satapathy SC, Dey N, Vijayarajan R (2018) DWT-PCA image fusion technique to improve segmentation accuracy in brain tumor analysis. In: Microelectronics, electromagnetics and telecommunications. Springer, pp 453–462
[19] Amin J, Sharif M, Gul N, Yasmin M, Shad SA (2019) Brain tumor classification based on DWT fusion of MRI sequences using convolutional neural network. Pattern Recognit Lett 129:115–122
[20] Sharif M, Amin J, Raza M, Yasmin M, Satapathy SC (2019) An integrated design of particle swarm optimization (PSO) with fusion of features for detection of brain tumor. Pattern Recognit Lett 129:129
[21] Kaus MR, Warfield SK, Nabavi A, Chatzidakis E, Black PM, Jolesz FA, Kikinis R (1999) Segmentation of meningiomas and low grade gliomas in MRI. In: International conference on medical image computing and computer-assisted intervention. Springer, Berlin, Heidelberg, pp 1–10
[22] Moon N, Bullitt E, Van Leemput K, Gerig G (2002) Model-based brain and tumor segmentation. In: ICPR, pp 528–531
[23] Prastawa M, Bullitt E, Ho S, Gerig G (2004) A brain tumor segmentation framework based on outlier detection. Med Image Anal 8(3):275–283
[24] Corso JJ, Sharon E, Yuille A (2006) Multilevel segmentation and integrated Bayesian model classification with an application to brain tumor segmentation. In: International conference on medical image computing and computer-assisted intervention. Springer, Berlin, Heidelberg, pp 790–798
[25] Moonis G, Liu J, Udupa JK, Hackney DB (2002) Estimation of tumor volume with fuzzy-connectedness segmentation of MR images. Am J Neuroradiol 23(3):356–363
[26] Lefohn AE, Cates JE, Whitaker RT (2003) Interactive, GPUbased level sets for 3D segmentation. In: International conference on medical image computing and computer-assisted intervention. Springer, Berlin, Heidelberg, pp 564–572
[27] Zhu Y, Yan Z (1997) Computerized tumor boundary detection using a Hopfield neural network. IEEE Trans Med Imaging 16(1):55–67

[28] Litjens G, Kooi T, Bejnordi BE, Setio AAA, Ciompi F, Ghafoorian M, Van Der Laak JA, Van Ginneken B, Sa´nchez CI (2017) A survey on deep learning in medical image analysis. Med Image Anal 42:60–88\
[29] Ravı D, Wong C, Deligianni F, Berthelot M, Andreu-Perez J, Lo B, Yang G-Z (2017) Deep learning for health informatics. IEEE J Biomed Health Inform 21(1):4–21.
[30] Huang G-B (2015), What are extreme learning machines? Filling the gap between Frank Rosenblatt's dream and John von Neumann's puzzle. Cogn Comput 7(3):263–278
[31] B. H. Menze, A. Jakab, S. Bauer, J. Kalpathy-Cramer, K. Farahani, J. Kirby, et al. "The Multimodal Brain Tumor Image Segmentation Benchmark (BRATS)", IEEE Transactions on Medical Imaging 34(10), 1993-2024 (2015) DOI: 10.1109/TMI.2014.2377694
[32] S. Bakas, H. Akbari, A. Sotiras, M. Bilello, M. Rozycki, J.S. Kirby, et al., "Advancing The Cancer Genome Atlas glioma MRI collections with expert segmentation labels and radiomic features", Nature Scientific Data, 4:170117 (2017) DOI: 10.1038/sdata.2017.117
[33] G. Gerig „Nonlinear anisotropic filtering of MRI data", IEEE Transactions on medical imaging 11.2 (1992), 221-232.
[34] M. A. Kabir, "A Rule Based Segmentation Approaches to Extract Retinal Blood Vessels in Fundus Image", American Scientific Research Journal for Engineering, Technology, and Sciences (ASRJETS), Vol 66 No 1, pp 202-224, 2020.
[35] W. Wan, L. Duan and Y. Wang, 'Fast Image Segmentation Using Two-Dimensional Otsu Based on Estimation of Distribution Algorithm', Journal of Electrical and Computer Engineering, p.1-12, Volume 2017.
[36] Chan TF, Vese LA (2001) Active contours without edges.IEEE Trans Image Process 10:266–277.
[37] M. A. Kabir, M. A. M. Khan, M. T. Islam, M. L. Hossain and A. F. Mitul, "Image compression using lifting based wavelet transform coupled with SPIHT algorithm," 2013 International Conference on Informatics, Electronics and Vision (ICIEV), Dhaka, 2013, pp. 1-4.
[38] Tian J. Hu Q. Ma X. Ha M. An Improved KPCA/GA-SVM Classication Model for Plant Leaf Disease Recognition Journal of Computational Information Systems , 2012, 18, 7737-7745.
[39] Melanie M. An Introduction to Genetic Algorithms A Bradford Book The MIT Press, 1999.
[40] A. Ziarati. A multilevel evolutionary algorithm for optimizing numerical functions" IJIEC 2 ; 419430 ; 2011
[41] H. John. Adaptation in Natural and Artificial Systems. Cambridge, MA: MIT Press. ISBN 978-0262581110; 1992.
[42] B. Oluleye. A. Leisa. LENG Jinsong. DIEPEVEEN Dean. Zernike Moments and Genetic Algorithm: Tutorial and Application. British Journal of Mathematics and Computer Science. 4(15): 2217-2236.
[43] M. Nasor and W. Obaid, 'Detection and Localization of Early-Stage Multiple Brain Tumors Using a Hybrid Technique of Patch-Based Processing, k-means Clustering and Object Counting', International Journal of Biomedical Imaging, Volume 2020, p 1-10.
[44] A. Gujar and C. M. Meshram, "Brain tumor extraction using genetic algorithm," International Journal on Future Revolution in Computer Science and Communication Engineering (IJFRSCE), vol. 4, no. 6, pp. 33–39, 2018.
[45] I. Kullayamma and A. Praveen Kumar, "Brain tumor segmentation by using ant colony optimization," International Journal of Scientific Research in Science and Technology, vol. 4, no. 8, pp. 62–69, 2018.
[46] Hussein AttyaLaftaEsraa Abdullah Hussein. Design a Classification System for Brain Magnetic Resonance Image. Journal of Babylon University, Pure and Applied Sciences. 21(8): p.1-8 (2013).
[47] Yusra Ibrahim Mohamed, Walaa Hussein Ibrahim, Ahmed Abdelrahman Ahmed Osman. MRI Brain Image Classification Using Neural Networks. In International Conference on Computing, Electrical and Electronics Engineering. Khartoum, Sudan, 26 - 29 August. IEEE: IEEE. 253-258 (2013).
[48] P. P. Gumaste and V. K. Bairagi, 'A Hybrid Method for Brain Tumor Detection using Advanced Textural Feature Extraction', Biomedical & Pharmacology Journal, Vol. 13(1), p. 145-157, March 2020.
[49] S, K. Bandyopadhyay, 'Detection of Brain Tumor Based on Extraction Feature Vectors', EC Emergency Medicine And Critical Care, 4.3 (2020): 01-09.